Efficient and Substantial DNA Lesions From Near 0 eV Electron-Induced Decay of the O_4-Hydrogenated Thymine Nucleotides: A DFT Study

Shoushan Wang, Changzhe Zhang, Peiwen Zhao, Yuxiang Bu[1]

School of Chemistry and Chemical Engineering, Institute of Theoretical Chemistry, Shandong University, Jinan, 250100, P. R. China

Supporting Information

The calculated structures, molecular orbitals, and spin density distributions of relevant molecules including initial reactants, transition state and products in the gas phase and aqueous phase.

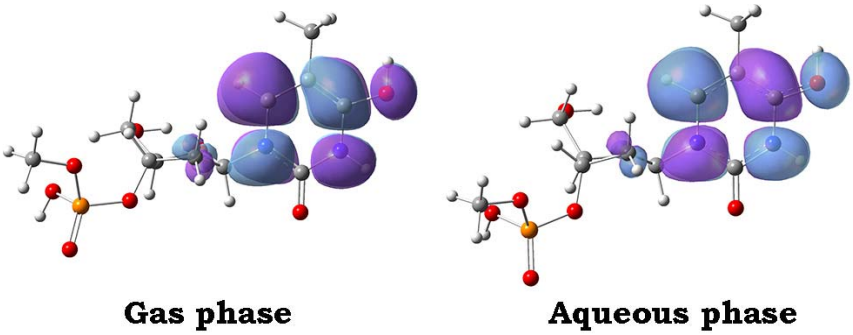

Figure S1. The HOMOs of 3′-dT(O4H)MPH in the gas phase and aqueous phase, respectively.

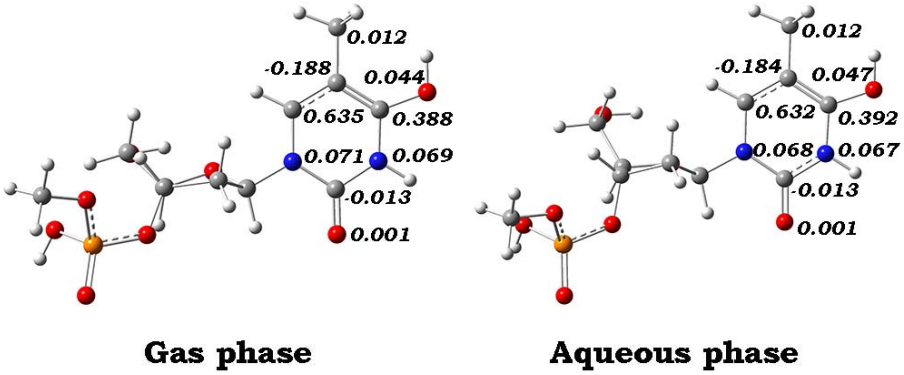

Figure S2. The spin density distributions on the base moiety of 3′-dT(O4H)MPH in the gas phase and aqueous phase, respectively.

* *The corresponding author: Yuxiang Bu, e-mail: byx@sdu.edu.cn*

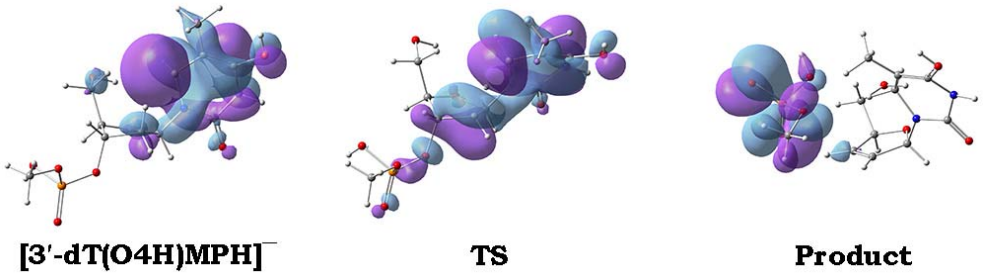

Figure S3. The HOMOs of relevant stationary points along the $C_{3'}$-$O_{3'}$ bond rupture pathway in the gas phase 3′-dT(O4H)MPH induced by EE attachment.

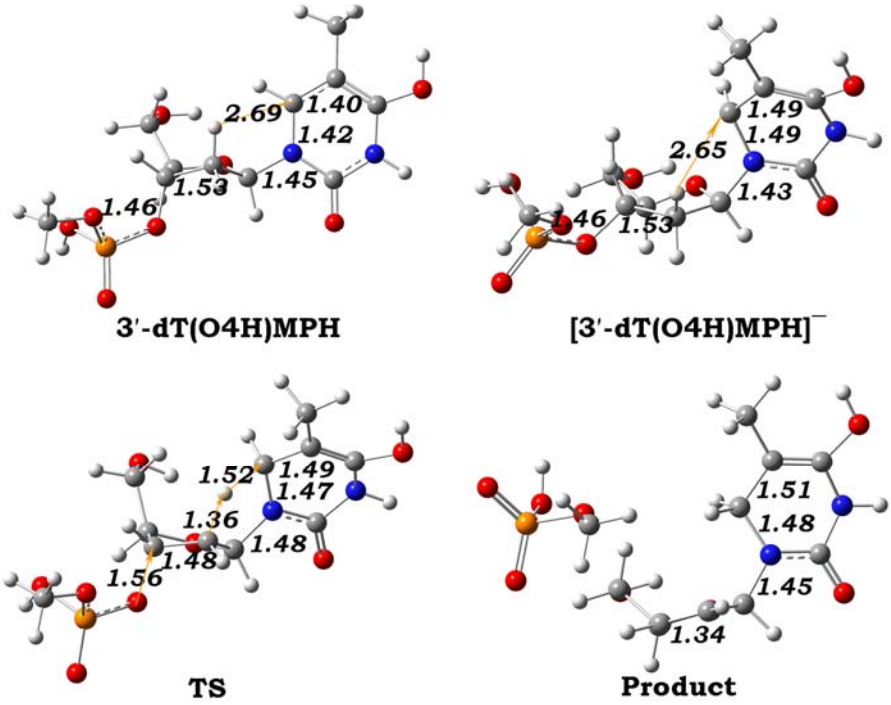

Figure S4. Optimized structures and selected geometrical parameters for stationary points along the $C_{3'}$-$O_{3'}$ bond rupture pathway in the aqueous phase 3′-dT(O4H)MPH induced by EE attachment. Distances are all in the unit of Å.

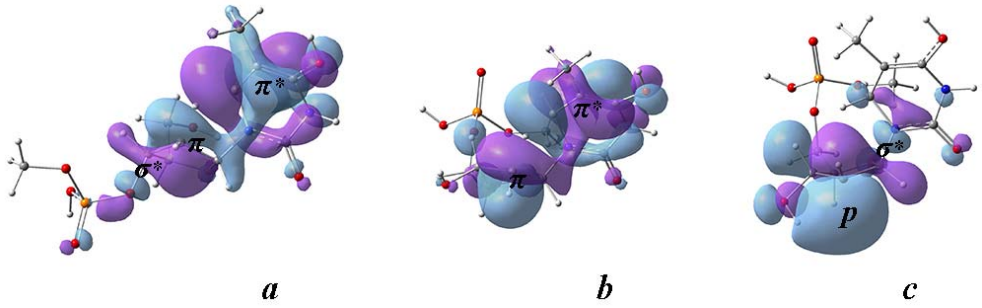

Figure S5. (*a*) The HOMO of the TS state along the aqueous phase $C_{3'}$-$O_{3'}$ bond rupture pathway in 3′-dT(O4H)MPH induced by EE attachment. (*b*) The HOMO of the TS1 state along the aqueous phase N_1-$C_{1'}$ bond rupture pathway in 5′-dT(O4H)MPH induced by EE attachment. (*c*) The HOMO of [5′-dT(O4H,C6H)MPH]$^-$ intermediate along the aqueous phase N_1-$C_{1'}$ bond rupture pathway in 5′-dT(O4H)MPH induced by EE attachment.

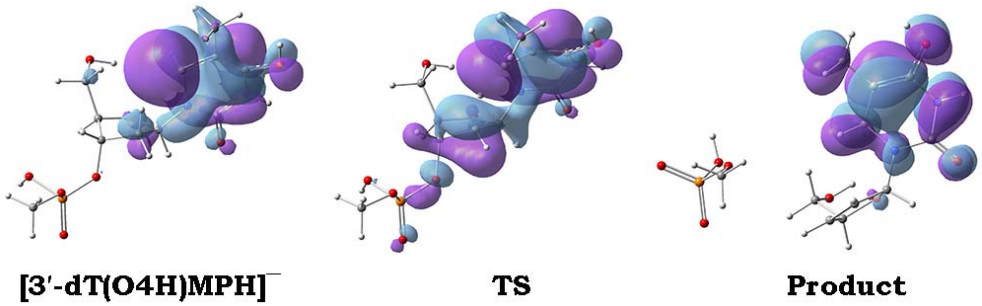

Figure S6. The HOMOs of relevant stationary points along the $C_{3'}$-$O_{3'}$ bond rupture pathway in the aqueous phase 3′-dT(O4H)MPH induced by EE attachment.

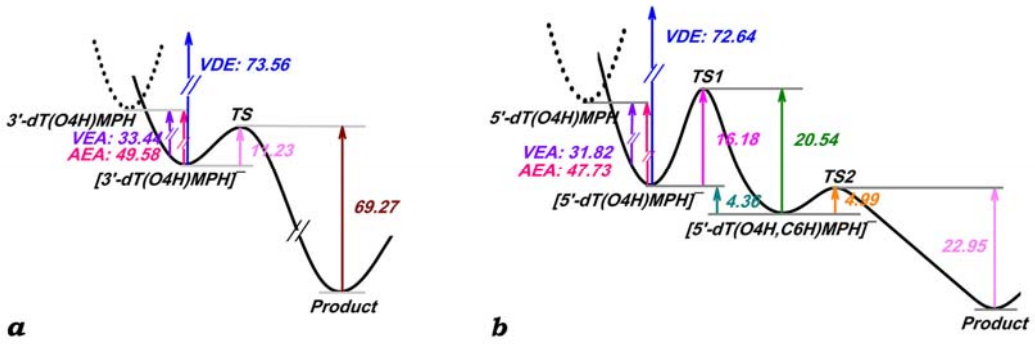

Figure S7. (*a*) The potential energy surface along the $C_{3'}$-$O_{3'}$ bond rupture pathway in the aqueous phase 3′-dT(O4H)MPH induced by EE attachment. (*b*) The potential energy surface along the N_1-$C_{1'}$ bond cleavage pathway in the aqueous phase 5′-dT(O4H)MPH induced by EE attachment. Energies are all in the unit of kcal/mol.

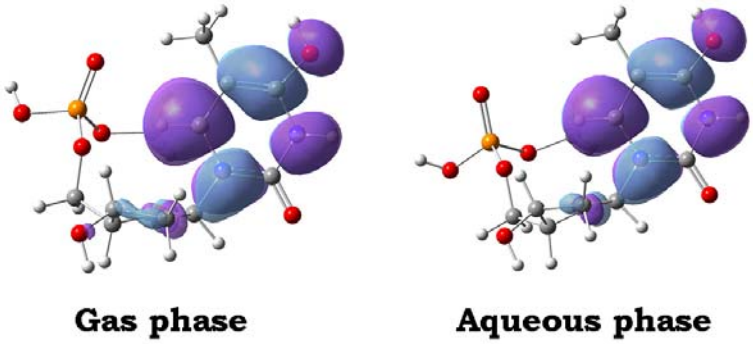

Figure S8. The HOMOs of 5′-dT(O4H)MPH in the gas phase and aqueous phase, respectively.

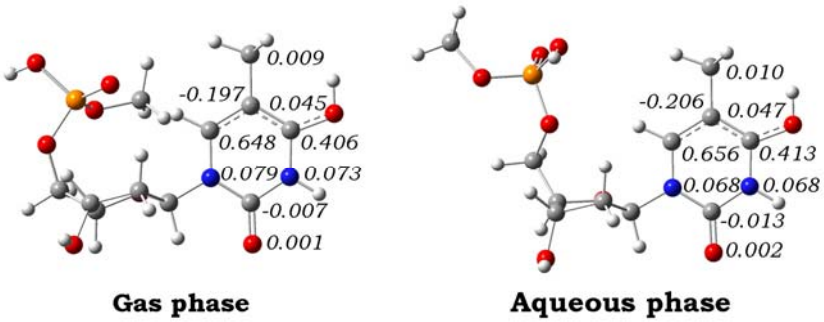

Figure S9. The spin density distributions on the base moiety of 5′-dT(O4H)MPH in the gas phase and aqueous phase, respectively.

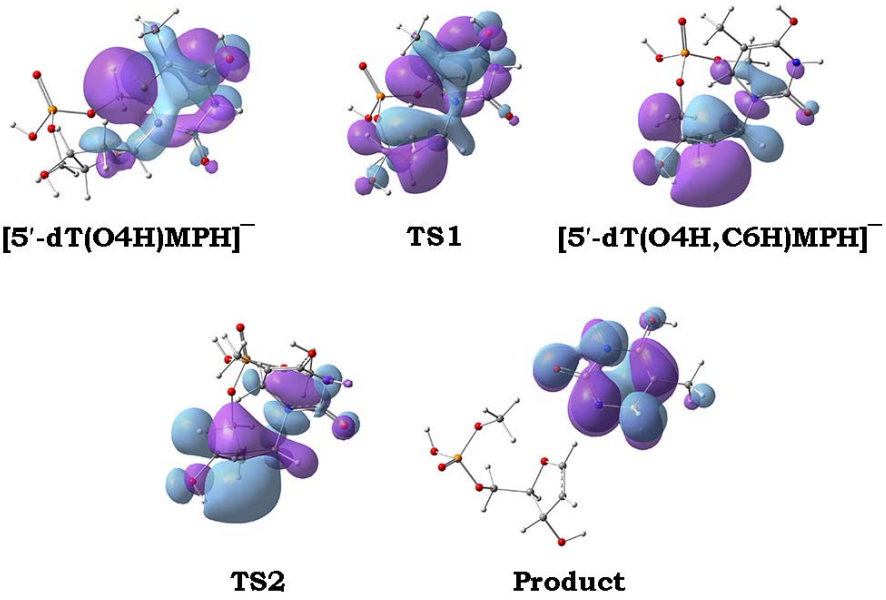

Figure S10. The HOMOs of relevant stationary points along the N_1-$C_{1'}$ bond cleavage pathway in the gas phase 5′-dT(O4H)MPH induced by EE attachment.

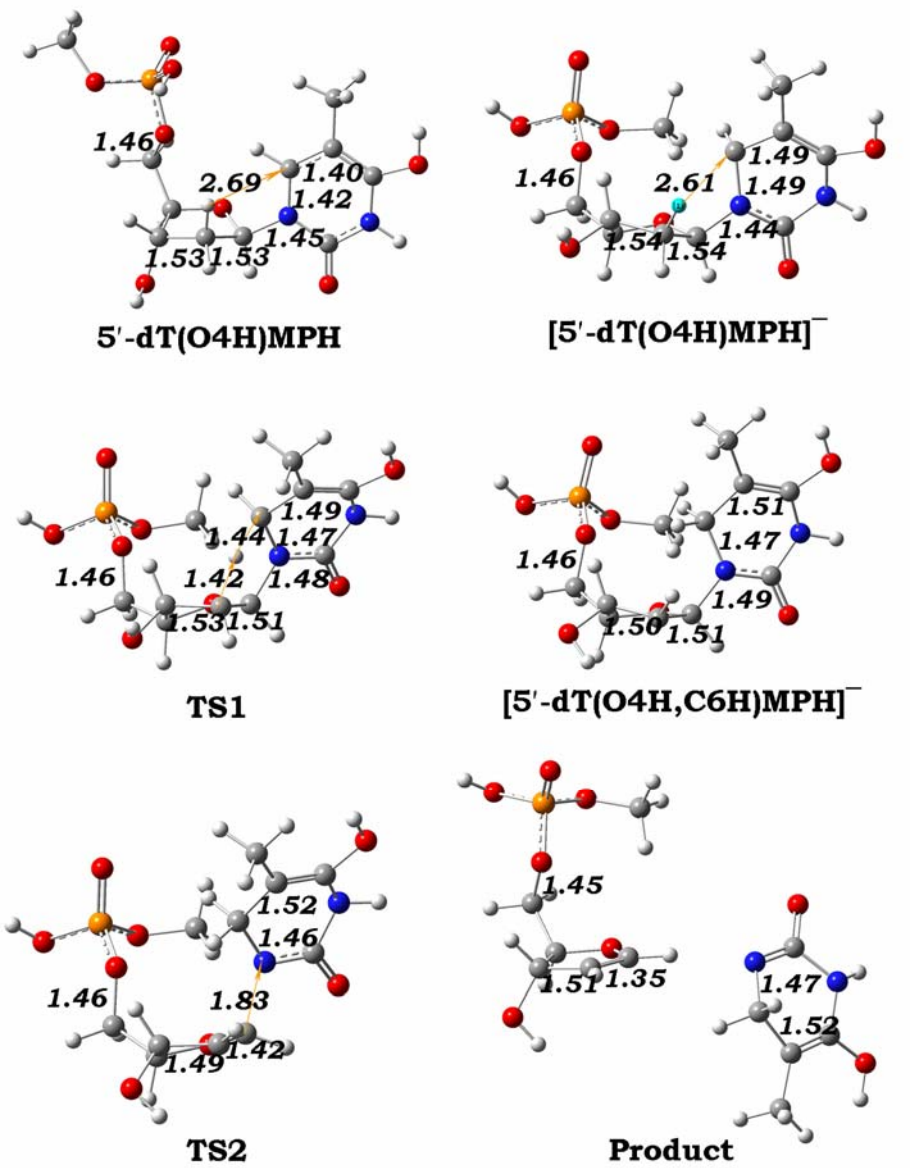

Figure S11. Optimized structures and selected geometrical parameters for stationary points along the N_1-$C_{1'}$ bond cleavage pathway in the aqueous phase 5′-dT(O4H)MPH induced by EE attachment. Distances are all in the unit of Å.

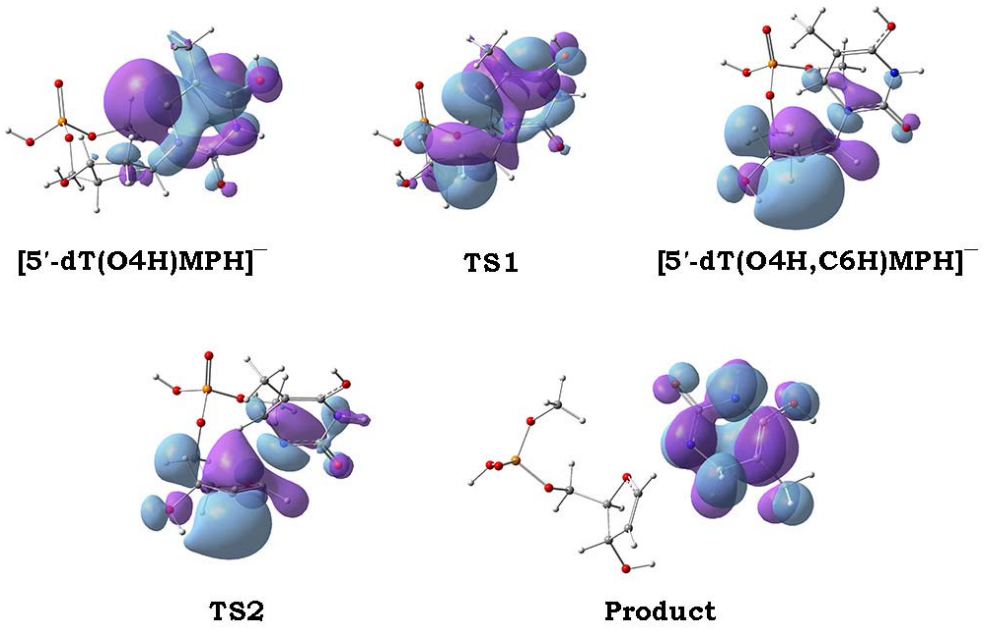

Figure S12. The HOMOs of relevant stationary points along the N_1-$C_{1'}$ bond cleavage pathway in the aqueous phase 5′-dT(O4H)MPH induced by EE attachment.